Agricultural and Forest Meteorology 347 (2024) 109910

Contents lists available at ScienceDirect

Agricultural and Forest Meteorology

journal homepage: www.elsevier.com/locate/agrformet

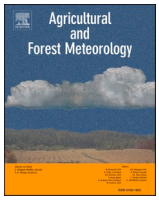

# Decadal variation and trend of boundary layer height and possible contributing factors in China

Congcong Li [a,b], Xuanze Zhang [b], Jianping Guo [c], Qiang Yu [a,b,*], Yongqiang Zhang [b,*]

[a] State Key Laboratory of Soil Erosion and Dryland Farming on the Loess Plateau, College of Natural Resources and Environment, Northwest A&F University, Yangling 712100, China
[b] Key Laboratory of Water Cycle and Related Land Surface Processes, Institute of Geographic Sciences and Natural Resources Research, Chinese Academy of Sciences, Beijing 100101, China
[c] State Key Laboratory of Severe Weather, Chinese Academy of Meteorological Sciences, Beijing 100081, China

ARTICLE INFO

*Key words:*
Boundary layer height
Contributing factors
Sensible heat flux
Latent heat flux
Wind speed
Interannual variability

ABSTRACT

Observational evidence has indicated a significant decline in the planetary boundary layer height (BLH) in China since the 2000s. However, the specific factors contributing to this decline have remained unclear. This study uses an approach based on partial derivative equation to investigate the individual and combined impacts of six potential land surface factors (sensible heat flux, latent heat flux, air temperature, specific humidity, wind speed, and vertical velocity) on the variation and trend of BLH in China from 2000 to 2016. The results reveal that wind speed predominantly influences BLH variation in most months, except for the period from June to August, where air temperature becomes the primary driver. Regarding the BLH trend, sensible heat flux plays a dominant role in most months and across various regions of China. However, during the June to August timeframe, the change in latent heat flux, driven by vegetation greening in northern China, becomes the primary factor influencing the BLH trend. These findings provide important insights for regional sustainable management and environmental protection, supporting policymakers and local administrations in China.

## 1. Introduction

The planetary boundary layer (PBL) represents the lowest layer of the atmosphere where exchange and transport processes of energy and water vapor occur between the air and land surface. It plays a crucial role in the overall atmospheric dynamics (Garratt, 1994; Stull, 2012; Zhu et al., 2018). The height of the planetary boundary layer, known as the boundary layer height (BLH), is an important metric that varies with latitude, altitude, and climate on Earth's surface (Seibert et al., 2000). Traditionally, BLH estimation involves height-resolved observations of temperature, specific humidity, and wind speed obtained from atmospheric soundings. Various methods have been developed utilizing observations such as radiosonde, LIDAR, and sodar to calculate the BLH (Beyrich, 1997; Guo et al., 2016b; Helbig et al., 2021; Mayor, 2017; Seidel et al., 2010; Su et al., 2017; Tang et al., 2021; Zhang et al., 2016a). Radiosonde measurements have been widely utilized in estimating BLH by considering the thermodynamic and dynamic conditions of the lower atmosphere, contributing to understanding its diurnal and seasonal variations (Liu and Liang, 2010; Seidel et al., 2010). Additionally, studies utilizing high-resolution micropulse LIDAR datasets have improved the spatial coverage of BLH and analyzed diurnal mixing layer height (Yang et al., 2013). Recent researches have focused on characterizing the climatology, and temporal and spatial variability of BLH in China with high temporal and spatial resolutions (Guo et al., 2016b).

The factors influencing BLH can vary across different temporal scales. In the short term, thermal instability and turbulence resulting from intense surface heating play a significant role in determining the height of the atmospheric boundary layer. At a seasonal scale, the BLH is influenced by seasonal shifts in large-scale pressure systems and changes in land surface friction due to phenology or drought. At annual to multiannual scales, changes in land surface conditions can affect the BLH. Investigating changes in BLH and identifying major contributing factors at seasonal and annual scales has been a focus of research over the past decade.

Table 1 provides a summary of several studies conducted in the last decade, focusing on the spatiotemporal characteristics and dominant factors influencing changes in BLH at seasonal to annual scales. For example, Xu et al. (2021a) utilized correlation analysis to investigate the

* Corresponding authors.
*E-mail addresses:* yuq@nwafu.edu.cn (Q. Yu), zhangyq@igsnrr.ac.cn (Y. Zhang).

https://doi.org/10.1016/j.agrformet.2024.109910
Received 17 June 2023; Received in revised form 12 January 2024; Accepted 25 January 2024
Available online 3 February 2024

**Table 1**
Summarizing the studies for investigating the changes and dominant factors on BLH.

| Study | Region | Method | Main objective | Key conclusion |
|---|---|---|---|---|
| Xu et al. (2021a) | China | Pearson correlation coefficient and regression lines | Correlation between soil moisture and *BLH* under different boundary layer regimes | There existed a negative correlation between SM and daytime *PBLH* under convective and neutral boundary layer |
| Sudeepkumar et al. (2020) | West coast of India | Regression analysis, two-way analysis of variance | Correlation between *BLH* and surface parameters, such as specific humidity, temperature, sensible & latent heat fluxes | The *BLH* was significantly decreased due to decrease in surface wind, and it was significantly correlated with surface parameters |
| Cao et al. (2020) | Sichuan Basin, China | Correlation analyses | Relationship between maximum *BLH* and temperature, geopotential height, sensible heat flux and wind | The sensible heat flux and wind shear were the main influencing factors to max boundary layer height on sunny days. |
| Darand and Zandkarimi (2019) | Iran | Correlation analyses | Relationship between *BLH* and air temperature and surface relative humidity over Iran | The variations of *BLH* showed a strong positive (negative) correlation with air temperature (surface relative humidity) |
| Guo et al. (2019) | China | Correlation analyses | Correlation between *BLH* and meteorological parameters | The *BLH* had a negative (positive) association with soil moisture, lower tropospheric stability and relative humidity (temperature) |
| Zhang et al. (2017) | China | Correlation analyses | Correlation between *BLH* and meteorological parameters | The *BLH* was found to be positively (negatively) associated with near-surface air temperature (humidity) |
| Wan et al. (2017) | East Asia | Correlation analyses | Correlation between *BLH* and sensible heat | The *BLH* had a positive correlation with sensible heat |
| Jousse et al. (2016) | Northeast Pacific | Weather research and forecasting numerical model | Relationship between *BLH* and sensible & latent heat fluxes | Sensible heat flux and latent heat flux are significantly correlated to *BLH* |
| Acs et al. (2014) | Carpathian Basin | Weather research and forecasting numerical model | Sensitivity of land cover and soil changes to *BLH* | PBL height differences caused by soil change were comparable with the PBL height differences caused by land cover change |
| Zhang et al. (2013) | Europe | Correlation analyses | Correlation between *BLH* and relative humidity and temperature | Daytime *BLH* variations showed a strong negative (positive) correlation with surface relative humidity (surface temperature) |
| Ma et al. (2011) | Northwest China | Weather research and forecasting numerical model | The sensitivity of soil moisture and surface albedo to *BLH* | The initial soil moisture and surface albedo were the influencing factors of *BLH* |
| This study | China | The partial derivative equation approach | Detection and attribution of *BLH* changes | Climate and vegetation changes both caused *BLH* declining in China |

relationship between soil moisture and BLH, finding a negative correlation under convective and neutral boundary layer conditions. Sudeepkumar et al. (2020) employed regression analysis and two-way analysis of variance to examine the influence of surface parameters, such as specific humidity, sensible heat flux, and latent heat flux, on BLH. Their findings indicated that BLH changes along the west coast of India from 1980 to 2018 were associated with surface specific humidity and energy exchange (i.e., sensible and latent heat flux). Jousse et al. (2016) employed the Weather Research and Forecasting model to explore the relationship between sensible heat flux, latent heat flux, and boundary layer thickness over the northeast Pacific region, observing a significant correlation between sensible and latent heat fluxes and BLH. Darand and Zandkarimi (2019) employed the correlation method to analyze the relationship between BLH and air temperature and relative humidity. Their results demonstrated a strong positive correlation between annual BLH variations and air temperature, as well as a strong negative correlation with surface relative humidity, attributing deeper convection and larger BLH to higher air temperature and lower relative humidity. Additionally, Acs et al. (2014) estimated BLH changes influenced by land cover and soil changes using the Weather Research and Forecasting model, and they found that differences in BLH caused by temperature and moisture changes in the soil were comparable to those caused by land cover changes. These studies collectively suggest that BLH changes are closely linked to near-surface meteorological variables, such as air temperature, specific humidity, and wind speed. Furthermore, the energy exchange at the surface layer (sensible heat flux and latent heat flux) and vertical velocity also impact BLH. Overall, the studies listed in Table 1 predominantly employ statistical methods to establish relationships between BLH and its potential contributing factors.

Investigating the contribution of different factors to the variation and trends of BLH in China is of great importance. Prior to 2000, China experienced significant soil erosion, degradation, and desertification on a large scale. To address these environmental challenges, various ecological programs have been implemented, resulting in extensive changes in land use and vegetation coverage (Qiu et al., 2017; Zhang et al., 2016b). Moreover, since 2000, rapid urbanization and substantial land use and land cover changes have occurred in China. These changes have influenced the water-energy balance between the atmosphere and land surface, including evapotranspiration, surface runoff, net radiation, sensible heat flux, and latent heat flux, consequently impacting regional climate and local precipitation processes (Zhang et al., 2021). It is reasonable to hypothesize that these significant modifications in land surface conditions have potentially altered the BLH by affecting surface energy fluxes and local climate conditions. Considering the BLH as the thickness of the lowest turbulent air layer, this study focuses on three categories of contributing factors: energy variables (sensible heat flux and latent heat flux), thermodynamic variables (specific humidity and air temperature), and dynamic variables (wind speed and vertical velocity) (Cao et al., 2020; Garratt, 1994; Zhang et al., 2014). Notably, previous research has indicated that BLH increases are associated with decreased surface relative humidity and increased surface temperature (Zhang et al., 2013). Air temperature and specific humidity reflect the overall energy and moisture content of the lower atmosphere, which have an impact on the stability of the lower troposphere (Guo et al., 2019; Raval and Ramanathan, 1989; Zhang et al., 2013). These six selected land surface variables (sensible heat flux, latent heat flux, surface air temperature, specific humidity, wind speed, and vertical velocity) are considered dominant factors contributing to BLH changes.

By exploring the relationship between BLH and these factors, this study aims to quantify their relative contributions to BLH changes in China. Specifically, this study focuses on examining the interannual variability and trends of the BLH in the northern, southern, and northwestern regions of China, and tries to quantify the relative contributions of several factors: sensible heat flux (*H*), latent heat flux (*LE*), surface air temperature (*T*), specific humidity (*SH*), wind speed (*WS*), and vertical

velocity (*VV*) (Fig. S1). The specific objectives of the study are as follows:

i) To uncover the annual variation and trend of the BLH and its possible contributing factors in China from 2000 to 2016;
ii) To compare the observed annual and seasonal variations in the BLH with those estimated by the possible contributing factors; and
iii) To investigate the contribution rate of the possible contributing factors to the trend of the BLH in China from 2000 to 2016.

## 2. Data and methods

### 2.1. Radiosonde measurements and relevant variables

The datasets used in this study to calculate the BLH at seasonal and annual scales from 2000 to 2016 were derived from radiosonde temperature profile measurements. These measurements were collected during cloud-free conditions and had an accuracy of ≤0.1 K in the troposphere (Bian et al., 2011). The datasets, including temperature, pressure, specific humidity, and wind speed, were obtained from the China Meteorological Administration (CMA) and recorded twice daily at 0000 UTC (0800 Beijing Time, BJT) and 1200 UTC (2000 BJT) (Chen et al., 2019b; Guo et al., 2016a). The PBL was classified into three categories: the convective boundary layer (CBL), neutral boundary layer (NBL), and stable boundary layer (SBL), based on the potential temperature profile. The CBL is predominant during the daytime, while the SBL dominates at nighttime. In this study, the BLH data at 1200 UTC (2000 BJT) were used to minimize the influence of surface-based inversions that commonly occur in the morning (Stull, 2012). The BLH data underwent strict quality control procedures and homogeneity tests, as detailed in Chen et al. (2019b). The bulk Richardson number (Ri) method was applied to estimate the BLH over China, which is applicable to both stable and convective conditions and has been previously used to compile BLH climatology in China. In addition, it is weakly dependent on the vertical resolution of sounding (Zhang et al., 2013). Furthermore, to account for terrain changes, all BLH values were referenced to a height above ground level.

The land surface variables *H, LE, T, SH, WS*, and *VV* were used from multiple datasets covering the period from 2000 to 2016. The *H* data were obtained from the Global Land Data Assimilation System (GLDAS) and provided a daily temporal resolution with a spatial resolution of 0.25° × 0.25° grid. The LE data were generated using a diagnostic biophysical model called PML-V2 (Zhang et al., 2019). It generated *LE* at 500 m and at 8-day resolutions by using GLDAS as climate force data and a Moderate-resolution Imaging Spectroradiometer (MODIS) leaf area index (Myneni et al., 2015). The *T, SH*, and *WS* data were collected from the China Meteorological Forcing Dataset (CMFD) with a spatial resolution of 0.1° × 0.1°. These variables were available at a daily temporal resolution (He et al., 2020). The *VV* data , representing vertical velocity, were obtained from ERA5-land with a daily temporal resolution and a spatial resolution of 0.25° × 0.25° (Hersbach et al., 2020).

To ensure consistency and comparability, all the land surface variables from the different datasets were calculated as annual or seasonal values within a 1° radius around the radiosonde site.

### 2.2. Method

#### 2.2.1. The partial derivative equation approach

This study aims to clarify the influence of six selected land surface variables from three categories of contributing factors to observed BLH based on statistical analysis. The partial derivative equation approach, as described by Roderick et al. (2007), is used to estimate the elasticities of multiple factors in a multivariate regression model, where the regression coefficients represent the relationships between the potential factors and the observed BLH. The chain rule is applied to describe the multivariate function that relates the observed BLH to the six possible contributing factors. The multivariate function can be expressed as follows:

$$BLH = f(H,\ LE,\ T,\ SH, WS,\ VV) \tag{1}$$

where *H, LE, T, SH, WS,* and *VV* are sensible heat flux, latent heat flux, surface air temperature, specific humidity, wind speed, and vertical velocity, respectively. The multivariate, nonparametric model (Eq. (1)) is developed by assuming that the absolute change in the *BLH* to its mean value during the study period is a linear combination of absolute changes in *H, LE, T, SH, WS,* and *VV* to their mean values. This can be estimated as:

$$dBLH = \frac{\partial BLH}{\partial H}dH + \frac{\partial BLH}{\partial LE}dLE + \frac{\partial BLH}{\partial T}dT + \frac{\partial BLH}{\partial SH}dSH + \frac{\partial BLH}{\partial WS}dWS + \frac{\partial BLH}{\partial VV}dVV \tag{2}$$

where $\frac{\partial BLH}{\partial H}$, $\frac{\partial BLH}{\partial LE}$, $\frac{\partial BLH}{\partial T}$, $\frac{\partial BLH}{\partial SH}$, $\frac{\partial BLH}{\partial WS}$, and $\frac{\partial BLH}{\partial VV}$ are the partial correlation coefficients of *H, LE, T, SH, WS* and *VV*. These regression coefficients of the possible contributing factors were estimated from 2000 to 2016.

When the absolute changes in the *BLH* and the six possible contributing factors in Eq. (2) are substituted by changes from their average values during the study period, Eq. (2) can be rearranged as follows:

$$\begin{aligned}\frac{BLH_i - \overline{BLH}}{BLH_i} = &\frac{\partial BLH}{\partial H}\frac{H_i}{BLH_i}\left(\frac{H_i - \overline{H}}{H_i}\right) + \frac{\partial BLH}{\partial LH}\frac{LH_i}{BLH_i}\left(\frac{LH_i - \overline{LH}}{LH_i}\right)\\ &+ \frac{\partial BLH}{\partial T}\frac{T_i}{BLH_i}\left(\frac{T_i - \overline{T}}{T_i}\right) + \frac{\partial BLH}{\partial SH}\frac{SH_i}{BLH_i}\left(\frac{SH_i - \overline{SH}}{SH_i}\right)\\ &+ \frac{\partial BLH}{\partial WS}\frac{WS_i}{BLH_i}\left(\frac{WS_i - \overline{WS}}{WS_i}\right) + \frac{\partial BLH}{\partial VV}\frac{VV_i}{BLH_i}\left(\frac{VV_i - \overline{VV}}{VV_i}\right)\end{aligned} \tag{3}$$

For convenience at seasonal (including spring, summer, autumn and winter) or annual scales, the following variables were defined:

$$\Delta x_i = x_i - \bar{x} \tag{4}$$

$$\Delta BLH_i = BLH_i - \overline{BLH} \tag{5}$$

$$\varepsilon_x = \frac{\partial BLH_i/BLH_i}{\partial x_i/x_i} \tag{6}$$

where $BLH_i$ represents the boundary layer height of a single season or year, $\overline{BLH}$ is the mean *BLH* in season or annual, $x_i$ represents the possible contributing factors of a single season or year, $\bar{x}$ is the their mean, and $\varepsilon_x$ represents the coefficient of elasticity for possible contributing factors at seasonal or annual scales (Zhang et al., 2023).

By applying the coefficients of elasticity for each driving factor at a seasonal or annual scale, we obtain:

$$\begin{aligned}\Delta BLH_{est} = &\left(\varepsilon_H\frac{\Delta H}{H} + \varepsilon_{LE}\frac{\Delta LE}{LE} + \varepsilon_T\frac{\Delta T}{T} + \varepsilon_{SH}\frac{\Delta SH}{SH} + \varepsilon_{WS}\frac{\Delta WS}{WS} + \varepsilon_{VV}\frac{\Delta VV}{VV}\right)\\ &\times BLH\end{aligned} \tag{7}$$

where $\Delta BLH_{est}$ is the estimated change in the *BLH* at a seasonal or annual scale. Based on the multivariate regression model (Eq. (7)), we obtain the seasonal or annual trend in $\Delta BLH$ as follows:

$$Tr_{\Delta BLHest} = \left( Tr\left(\varepsilon_H \frac{\Delta H}{H}\right) + Tr\left(\varepsilon_{LE} \frac{\Delta LE}{LE}\right) + Tr\left(\varepsilon_T \frac{\Delta T}{T}\right) + Tr\left(\varepsilon_{SH} \frac{\Delta SH}{SH}\right) + Tr\left(\varepsilon_{WS} \frac{\Delta WS}{WS}\right) + Tr\left(\varepsilon_{VV} \frac{\Delta VV}{VV}\right) \right) \times BLH \quad (8)$$

where *Tr* presents the estimated trend of the variables from 2000 to 2016 at a seasonal or annual scale.

#### 2.2.2. Empirical mode decomposition

To examine the temporal trends of the studied variables, the empirical mode decomposition (EMD) algorithm, introduced by Wang et al. (2010), was employed. The EMD algorithm allows for the decomposition of a signal, x(*t*), into intrinsic mode functions (IMFs) and a residual component, which filters out the underlying trend. Through an iterative process, the EMD algorithm decomposes the fluctuations or residuals of different scales present in the original signal data, generating a series of data sequences with distinct characteristic scales.

The EMD algorithm is represented as follows:

$$x(t) = \sum_{i=1}^{N} IMF_i(t) + r_N(t) \quad (9)$$

where *N* denotes the number of IMFs obtained from the decomposition process.

In this study, the trend filtering, represented by $r_N(t)$, was analyzed for the BLH and the possible contributing factors over the period from 2000 to 2016 in different regions of China.

#### 2.2.3. Relative contribution of possible contributing factors

The relative contribution of the possible contributing factors to the variation in the *BLH* (i.e., $\Delta BLH$) is calculated from coefficients of elasticity, as follows:

$$CR_x = \frac{|\varepsilon_x|}{\sum_{k=1}^{6} |\varepsilon_x|} \quad (10)$$

where *CR* is the contribution rate, and the sum of the relative contribution equals 1.0.

The relative contribution of possible contributing factors to $Tr_{\Delta BLHest}$ can be seen below:

$$CR_{Tr_x} = \frac{|Tr_x|}{\sum_{k=1}^{6} |Tr_x|} \quad (11)$$

where *x* represents the variables of the six possible contributing factors, and the sum of the relative contribution equals 1.0.

## 3. Results

### 3.1. The annual mean and trends in the BLH and possible contributing factors in China

Fig. 2a-g presents a summary of the spatial patterns of the annual mean *BLH, H, LE, T, SH, WS,* and *VV* data across the research regions from 2000 to 2016. It is widely acknowledged that BLH and its potential contributing factors exhibit spatial heterogeneity across mainland China. The annual means of *BLH, H, WS,* and *VV* demonstrate a distinct spatial pattern of "High in the West and Low in the East," while the annual means of *LE, T*, and *SH* show a pattern of "High in the East and Low in the West."

Fig. 2h-n illustrates the spatial pattern of linear trends in *BLH, H, LE, T, SH,* and *WS* from 2000 to 2016. Interestingly, the trends in *BLH, H* and *VV* have decreased over most of the studied areas, whereas other variables generally exhibit increasing trends. These findings indicate a strong correlation between BLH changes and the six potential contributing factors.

### 3.2. The temporal disparity in BLH and its possible contributing factors

To analyze the dependence of *BLH* on causal factors, we examine three regions separately: northern, southern, and northwest China (Figure S1). Fig. 3 illustrates the temporal variations in *BLH, H, LE, T, SH, WS,* and *VV* in these regions from 2000 to 2016.

Observing Fig. 3, it is evident that the BLH in all three regions has decreased, exhibiting similar trends derived from EMD trend filtering. The *H* data shows decreasing trends across all regions, while the *LE* data indicates an increase, particularly in northern China. The air temperature trend is slightly positive, while the *SH* and *WS* trends initially decrease and then show later increases. The vertical velocity trend follows a similar pattern to the BLH trend in northwestern China, while the vertical velocity first increases and then later decreases in southern or northern China.

The relative importance of each contributing factor in the decrease in BLH in China from 2000 to 2016 is further quantified. This analysis involves utilizing the six possible contributing factors and estimating the BLH in China through the use of the partial derivative equation approach (Section 2.2.1). The results demonstrate that the annual and seasonal variations in the estimated BLH, based on the possible contributing factors, align well with the observed BLH in China, exhibiting a determination coefficient ($R^2$) above 0.4. Regression analysis reveals that the coefficients of *H, LE*, and *WS* in relation to *BLH* are negative. Conversely, the elasticity coefficients of *T* and *VV* exhibit a positive correlation with BLH. Regarding *SH*, the coefficient is negative for all regions of China, except for southern China (Figure S1).

### 3.3. The possible contributing factors for the change in BLH

Based on the estimated elasticities of the possible contributing factors, we use the observation factors to estimate the $\Delta BLH$ on an annual or seasonal scale. Figs. 4a-e show that the estimated Δ BLH (Eq. (7)) performs well against annual and seasonal observations. For the annual scale, the correlation (R) between the observed and estimated $\Delta BLH$ is above 0.75 ($p < 0.001$) in all three regions. For example, in spring (i.e., MAM in Fig. 4b), the R values are all similar at 0.75, 0.74 and 0.69 in northern, southern, and northwestern China, respectively. In summer (JJA), the R value is found to be the highest in northern China (0.76), followed by southern China (0.75) and northwestern China (0.73). In autumn (SON), the R values are the highest in southern China (0.80), followed by northwestern China (0.79) and northern China (0.78). Last, in winter (DJF), the R value is the highest in northern China (0.75) compared to the other regions (0.72). It is worth mentioning that the estimation of ΔBLH in northern China exhibits better accuracy than that in other regions, expect for in SON (autumn) seasons. Nonetheless, even in regions where the estimation may not be as accurate, there is still a satisfactory level of agreement between the observed and estimated

ΔBLH, with an R-value exceeding 0.69. This implies that the possible contributing factors used in this study can largely be used to attribute variations in the *BLH*.

The relative contribution of each contributing factor to the *ΔBLH* is further quantified. The summed contribution of *T, SH,* and *WS* to the *ΔBLH* in China is above 62 % at both annual and seasonal scales (Fig. 3f). The dominant factors of the different regions over the same periods are similar. For the annual scale, the most dominant factor is *T* (36 %) in southern China, but *SH* is dominant in mainland China (27 %), northern China (28 %), and northwest China (32 %). For mainland China and at a seasonal scale, the dominant factor is *T* (27∼38 %) in most seasons, but *WS* (24∼30 %) in JJA and DJF. Furthermore, the dominant factor is *T* (35∼45 %) in JJA in northern China, southern China and northwest China. The dominant factor is *WS* (25∼27 %) in northern and northwest China, but *T* (38 %) over SON in southern China. The dominant factor is *WS* (33 %) over DJF in northern and southern China, but *SH* (34 %) in northwestern China. The dominant factors over MAM are *WS* (29 %), *T* (35 %) and *WS* (32 %) in northern, southern and northwestern China, respectively.

Fig. 5a-e illustrates a comparison between the observed *ΔBLH* trends and the estimated trends at annual and seasonal scales. Overall, the trend of the estimated *ΔBLH* ($Tr_{\Delta BLHest}$) is strongly positively correlated to that of the observed *ΔBLH* ($Tr_{\Delta BLHob}$). The R value between the two is larger than 0.79 ($p < 0.001$) at both annual and seasonal scales. $Tr_{\Delta BLHest}$ performs best from SON and worst from MAM. At seasonal scales, the estimated $Tr_{\Delta BLHest}$ performs similarly in the three regions. The R value in southern China is $> 0.93$, in northwest China it is between 0.88∼0.95, and in northern China, it is $> 0.97$ in all seasons except for MAM ($R = 0.79$) (Figs. 4b-e). This study also analyzes the contribution of the six possible contributing factors at annual and seasonal scales. Overall, the summed contribution of *H* and *WS* to $Tr_{\Delta BLHest}$ over China is between 45∼66 % in different regions at annual and seasonal scales. The dominant factor for $Tr_{\Delta BLHest}$ is *WS* or *H* (above 17 %) at either annual or seasonal scales in all of, northern, southern and northwestern China. It is interesting to note that the contribution of *LE* is largest (36 %) in northern China in JJA, which is much higher than that in southern and northwestern China.

## 4. Discussion

It is complex and difficult to detect the causality for the variability and trends in the *BLH* in China, where land cover and land use conditions have undergone dramatic changes. This can be attributed to urbanization, economic development and the implementation of ecological projects over the last few decades (Chen et al., 2019a). The effects of land surface changes on the regional climate could be important at a regional scale. Changes in the land surface regulate the climate by mediating energy and water balances at the land surface. As shown in Fig. 1, land surface changes or vegetation coverage changes can impact the water vapor transported to the atmosphere, including changes in regional atmospheric humidity, air temperature, and hydrological patterns (Liang et al., 2015).

Previous studies have shown that vegetation greening has led to an increase in evapotranspiration (or latent heat flux). The incoming solar radiation is balanced by the energy released from the land surface. Net radiation is partitioned into latent heat flux, sensible heat flux and soil heat flux. Soil heat flux is negligible at seasonal to monthly scales. Therefore, the land surface conditions strongly influence the proportion that is returned as latent heat versus sensible heat fluxes (Li et al., 2020; Zhang et al., 2021). Furthermore, large-scale vegetation greening has a positive effect on regional precipitation, including an increase in the total amount of rainwater resources, which shows that vegetation greening accelerates the global water cycle (Xu et al., 2021b; Zhang et al., 2021). In addition, changes in the land surface can also change the surface roughness and turbulence patterns that influence wind speed and vertical velocity (Hernandez et al., 2015; Zha et al., 2017) .

Using the *BLH* derived from the record of high-resolution radiosonde measurements from 2000 to 2016, this study investigated the variability and trend of *BLH* and possible surface contributing factors in China. This study described the *BLH* and six possible land surface contributing factors over China for the annual mean and trend separately. All parameters exhibit a distinct west to east gradient. It was found that in wet regions of eastern China, the *BLH* is lower than that in drylands of western China largely covered by grasslands and bare soil (Guo et al., 2019; Zhang et al., 2017). The *BLH* and *H* show decreasing trends at most stations while other variables mostly show increasing trends. To quantify the temporal variations in *BLH* and possible land surface contributing factors, measurements of possible land surface contributing factors are analyzed in tandem with those of BLH. We can observe that the *BLH* is decreased in all three regions. In addition, the range of *BLH* decrease in northwestern China is larger than that in northern and southern China. Surface possible contributing factors have large interannual fluctuations. For example, the air temperature and specific humidity both increased in China. The boundary layer traps the temperature and moisture at the low levels, and this enhanced specific humidity and latent heat flux give rise to heavy rainfall which may lead to the occurrence of vulnerable situations such as floods and landslides.

It is interesting to discuss how air temperature and specific humidity affect changes in *BLH*. First, the boundary layer is the closest to the earth's surface, and its height is strongly influenced by the stability characteristics of the surrounding air (Stull, 2012). Elevated surface temperatures induce the ascent of warm air, fostering vertical growth within the atmospheric boundary layer. Higher air temperature and lower humidity tend to render the boundary layer more unstable, facilitating vertical mixing and an increase in height (Guo et al., 2019). By integrating air temperature and specific humidity into the 6-variable partial derivative equation approach, we witness an enhancement in its performance, reflected in an average increase of $R^2$ value by 0.10 when compared to the 4-variable approach. Second, air temperature and specific humidity are more than a proxy for stability. We consider using lifting condensation level (LCL), an integrated variable including temperature and humidity, to simulate the variability in boundary layer height. For consistency, we follow Lawrence (2005) to diagnose the LCL using surface temperature and surface dew point temperature. We then replace air temperature and specific humidity with LCL that is obtained from CMFD data and the Modern-Era Retrospective analysis for Research and Applications, Version 2 (MERRA-2) data, respectively, and conduct the partial derivative equation analysis. The result shows that using LCL (obtained from CMFD or MERRA-2) is poorer than using air temperature and specific humidity, with a decrease of $R^2$ by about 0.04. In short, our results strongly imply that the variability of air temperature and specific humidity significantly governs the fluctuations in surface fluxes and the growth of the boundary layer. Consequently, these factors also exert a discernible influence on the variations observed in air temperature and specific humidity levels.

Interestingly, this study shows that *LE* has different contributions to the *BLH* in different regions of China. In northern China, the contribution rate of *LE* is higher than that in southern and northwestern China in most seasons, especially in summer. To further investigate the impact of *LE* on BLH in China, we conducted a similar analysis using *LE* data from ERA5-land. The results indicate a strong positive correlation between the estimated change in BLH (*TrΔBLHest*) using *LE* from ERA5-land and the observed change in BLH (*TrΔBLHob*), with an R-value larger than 0.90 ($p < 0.001$). However, we found that the contribution ratio of *LE* from ERA5-land to the overall analysis, both on an annual and seasonal scale, is relatively smaller compared to *LE* from PML-V2, especially during the spring and summer seasons (refer to Figs. 5 and S6). This also demonstrates the benefit of using remotely sensed leaf area of to obtain reasonable *LE* estimates. The large role of *LE* from PML-V2 plays in northern China can be attributed to the fact that the vegetation coverage has largely increased over the last two decades, following the implementation of several national policies/ecological projects (Chen et al.,

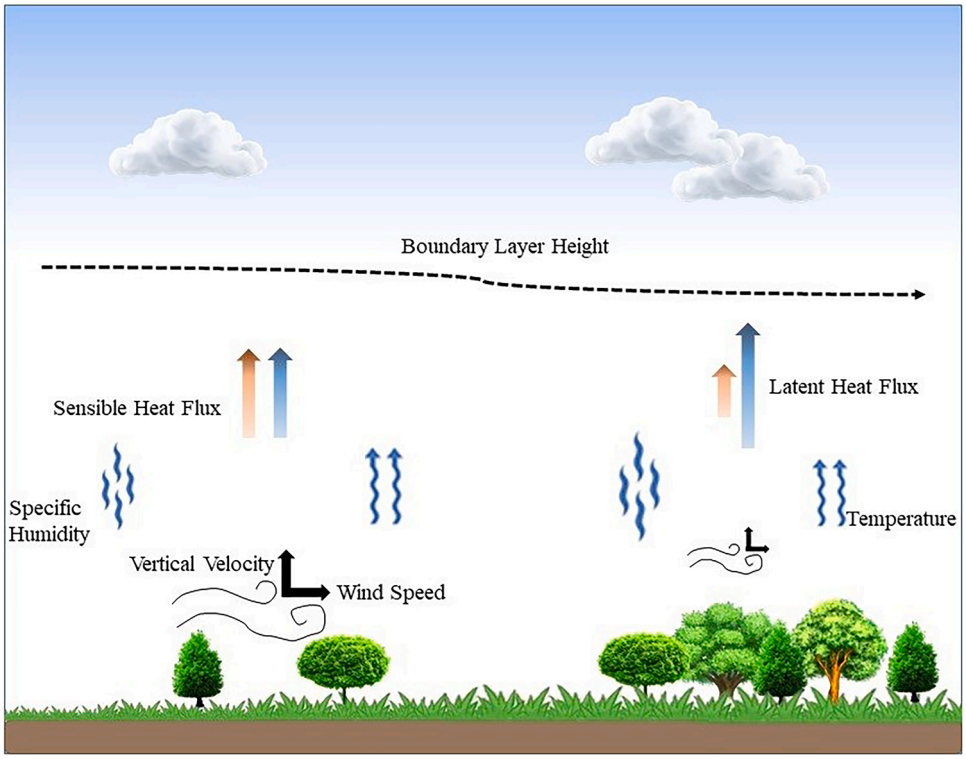


**Fig. 1.** A schematic diagram depicting the main contributing factors that influence the boundary layer height. These factors include sensible heat flux (*H*), latent heat flux (*LE*), surface air temperature (*T*), specific humidity (*SH*), wind speed (*WS*), and vertical velocity (*VV*).

2019a; Zhang et al., 2016b).

The study further analyzed the relationship between the annual leaf area index (*LAI*) and annual *LE* and found a strong relationship between the two in northern China (Figure S2). The tendency of co-increasing *LAI* and *LE* is even stronger at a summer scale than at an annual scale (Figure S3), demonstrated by $R = 0.85$ in northern China at the summer scale, compared to $R = 0.62$ at an annual scale. These results demonstrate that increase in LAI strongly enhances *LE*, particularly in northern China in summer. This further confirms that large-scale vegetation greening in northern China has caused a strong increase in *LE* (Chen et al., 2020; Zhang et al., 2017). Consequently, the increase in LE has led to a decrease in the sensible heat transfer from the land surface to the atmosphere, which plays a major role in controlling the decrease in the *BLH* in summer (Fig. 5f). This interaction has contributed significantly to the decline in BLH. This has resulted in a negative indication of regional environmental pollution management (Wang et al., 2013; Zhang et al., 2017).

More importantly, this study pioneered the examination of the relative contribution of possible surface contributing factors to the variability and trend of *BLH* at annual and seasonal scales in China with the partial derivative equation approach. The results from this study show that the annual and seasonal *BLHs* estimated by *H, LE, T, SH,* and *WS* correspond well with the observed *BLH* (Figure S1). This can especially be seen in northern China, which suggests that the possible surface contributing factors can explain most of the *BLH* changes in China. For the temporal variability in *BLH*, the summed contributions of *T, SH* and *WS* are above 62 % in all of, northern, southern and northwest China. However, it should be noted that the factors are not consistent in different seasons and regions. Overall, the *ΔBLH* over China is mainly controlled by *WS* in most seasons, but by *T* in summer (Miao et al., 2017; Xue et al., 2019). For the annual trend in *BLH*, the summed contributions of *WS, H* and *SH* are larger than 68 % in all of, northern, southern and northwestern China. Furthermore, the *WS* increased after 2010, yet the sensible heat flux decreased with time in China, the thermal turbulence caused by the thickness of the boundary layer decreased, and the height of the boundary layer decreased (Fig. 3). The possible contributing factors (except for WS) played an important role in the trend of the *BLH* after 2010. The contribution of surface possible contributing factors to the variability and trend of *BLH* in China is different in each period. Overall, this study concisely estimated the variability and trend of *BLH* and directly examined the relative contribution of possible surface contributing factors to the *BLH*.

It is worth reiterating that the possible contributing factors used in this study include not only those for atmospheric circulation processes, but also those for local energy and water cycling. For instance, the air temperature is the result of local energy cycling and large scale advection. These changes are expected to provide underlying feedback to the *BLH,* by changing its surface possible contributing factors (Mccumber and Pielke, 1981; Prueger et al., 1996; Raval and Ramanathan, 1989; Zhang et al., 2013). Other factors that can affect the *BLH* are soil moisture and soil temperature via the exchange of water and heat fluxes between the land surface and the atmosphere. Another contributing factor is atmospheric aerosols, which has a negative impact on the *BLH* (Malavelle et al., 2011). Nevertheless, its impact such as the increasing temperature difference between the middle atmosphere and surface can be complexly coupled with the six possible contributing factors in this study. Above all, this study using a partial derivative equation approach with possible surface contributing factors can sufficiently explain the variability and trends of *BLH* in China.

Despite the solid performance, we need to discuss the uncertainty or limitations of this study. First, this study estimates the variation and trend in *BLH* by the six possible contributing factors. It is possible that the uncertainty in the variables selected could influence the accuracy of the results. We noted that the *BLH* is complexly influenced by various factors including their interplay (Brugger et al., 2018; Wang et al., 2016). Therefore, this study used all six variables (*LE, H, T, SH, WS* and *VV*) from the energy, thermodynamic and dynamic effects as possible contributing factors. To reduce the effect of possible interplays of these factors, we also used four variables (*LE, H, WS* and *VV*) and five variables (*LE, H, T, WS* and *VV*) for the same analysis. We found that the BLH

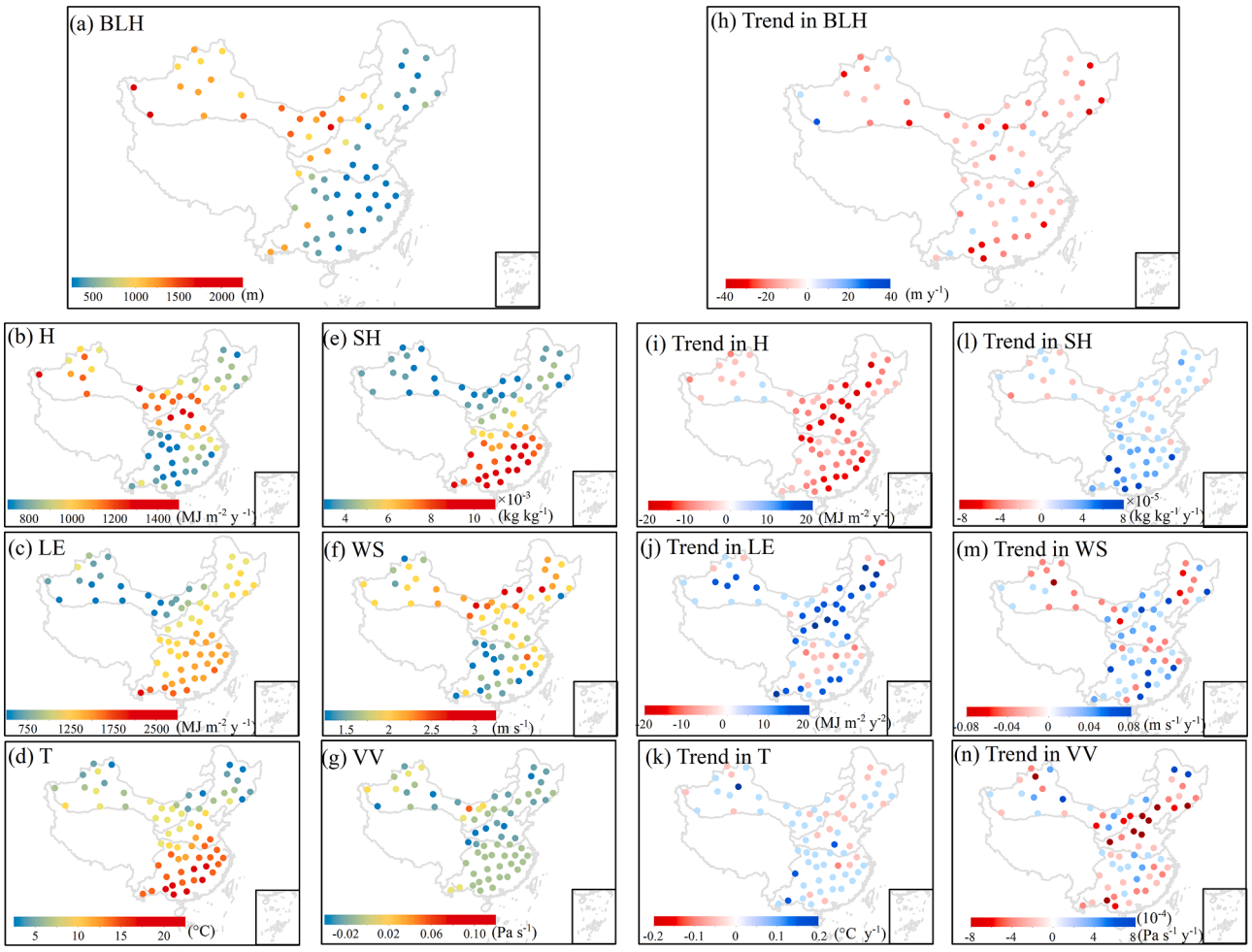


**Fig. 2.** The spatial distribution of the annual mean (a-g) and annual trend (h-n) in *BLH, H, LE, T, SH, WS,* and *VV* over 68 stations in China during 2000–2016. The abbreviations *BLH, H, LE, T, SH, WS,* and *VV* are the boundary layer height, sensible heat flux, latent heat flux, air temperature, specific humidity, wind speed, and vertical velocity, respectively.

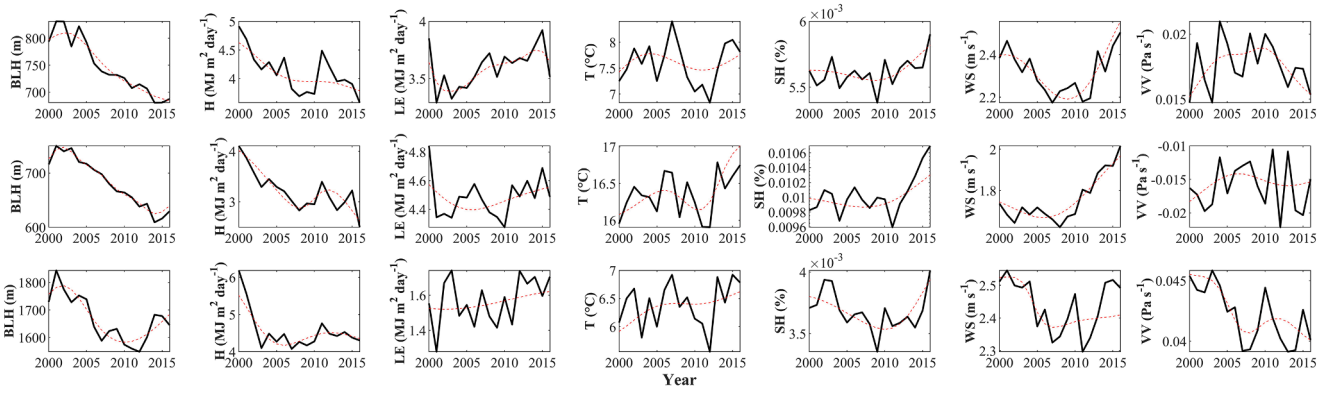


**Fig. 3.** Time series of the annual *BLH, H, LE, T, SH* and *WS* over the three regions of China at 2000 BJT from 2000 to 2016. The black curves represent the annual time series, while the red curves indicate the residual or trend filtering obtained through empirical mode decomposition (EMD) using Eq. (9). The panels in the top, middle, and bottom rows correspond to northern China, southern China, and northwest China, respectively. .

estimated by six variables was noticeably better than that estimated using four variables or five variables (Figure S4). This gives us confidence in using six possible contributing factors to estimate the variation and trend in *BLH* at a seasonal or annual scale (Figure S5). Second, this study has a limitation in that the direct aerosol impact on the *BLH* has not been included as there are no large-scale aerosol observations available (Ou et al., 2021; Rihani et al., 2015; Xu et al., 2021a). Third, this study is subject to the limited spatial and temporal coverage of good quality radiosonde measurements. This is because in the past, only several observational studies have been conducted on the long-term *BLH* trend at a regional scale (Guo et al., 2019). Fourth, this study ignores the process analysis on how the possible contributing factors affect the *BLH*, such as the subsidence or changes in free tropospheric conditions that are influenced by the surface possible contributing factors (Zuidema

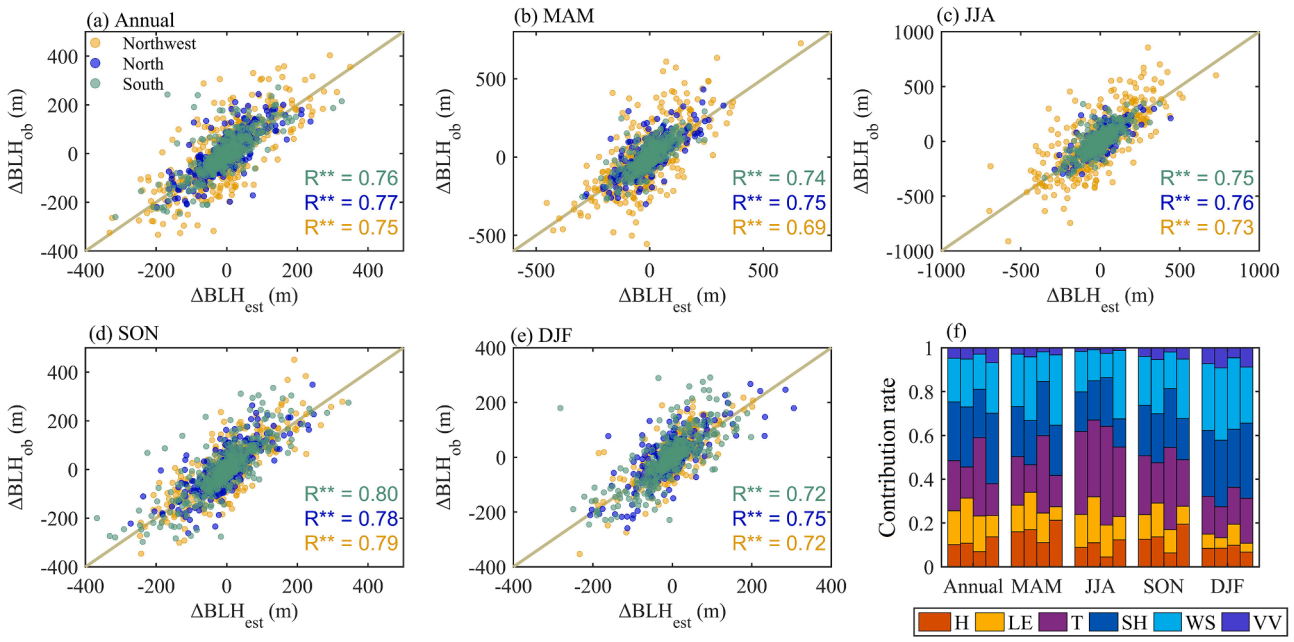


**Fig. 4.** The relationship between the *ΔBLH* estimated ($\Delta BLH_{est}$) and the observed ($\Delta BLH_{ob}$) in (a) annual, (b) MAM, (c) JJA, (d) SON, and (e) DJF. Where MAM, JJA, SON and DJF present March-to-May, June-to-August, September-to-November and December-to-February respectively. Furthermore, the symbols in blue, green, and yellow stand for northern, southern and northwest China; the symbol ** is a significance level (*p*) smaller than 0.001 and the symbol * is a *p* value smaller than 0.05. (f) shows the contribution rate of each of the following selected factors of *ΔBLH* from 2000 to 2016 in China. In (f), the four columns from left to right within each panel represent whole, northern, southern and northwestern China, respectively. .

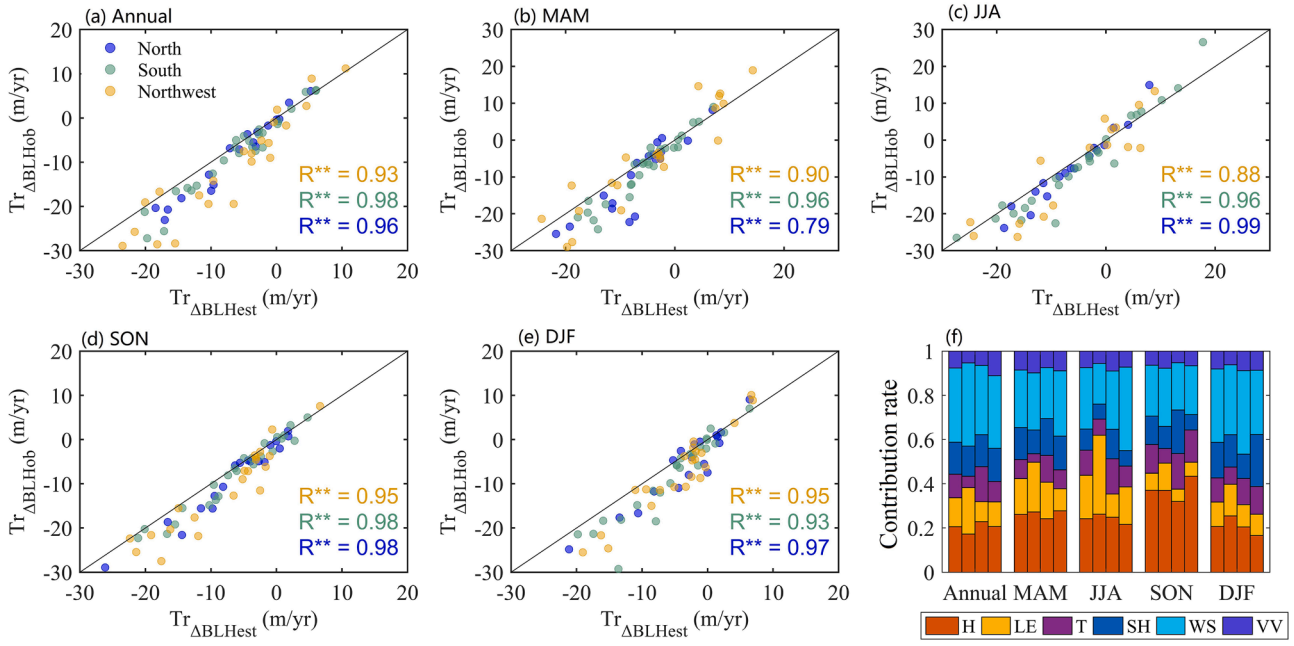


**Fig. 5.** In (a)-(e), the relationship between the trends of the estimated ($Tr_{\Delta BLHest}$) and the observed *ΔBLH* ($Tr_{\Delta BLHob}$) annually, and from MAM, JJA, SON, and DJF is shown. The symbols in blue, green and yellow represent northern, southern and northwest China, respectively; the symbol ** is a significance level (*p*) smaller than 0.001 and the symbol * is a *p* value smaller than 0.05. In (f), the contribution of the selected factors to $T_{\Delta BLHest}$ from 2000 to 2016 in China is shown. The four columns from left to right within each panel represent whole, northern, southern, and northwestern China, respectively.

et al., 2009).

In summary, this study reveals that vegetation changes play a role in decreasing *BLH*, but more details about the links between land use and land cover change and *BLH* are still not clear. More insights should be provided on the mechanism and process-based model simulation of the relationship between the two in the future. Despite the uncertainties and limitations, this study provided an improved understanding of the changes in the *BLH* and the major possible contributing factors in China.

## 5. Conclusions

Investigating the variability and trends of boundary layer height (BLH) is a challenging yet crucial scientific inquiry in China, particularly due to significant land surface changes that have occurred since the

2000s. This study comprehensively examines six potential surface contributing factors (sensible heat flux, latent heat flux, air temperature, specific humidity, wind speed, and vertical velocity) and their impacts on the observed BLH in China, which has exhibited a noticeable overall decrease, as well as in northern, southern, and northwest China, from 2000 to 2016.

The results of the study suggest that the six potential contributing factors can largely account for the observed changes in BLH, especially in northern China. Among these factors, wind speed emerges as the dominant factor influencing the variability of BLH, while specific humidity plays a significant role in the decreasing trend. Additionally, the declining trend of BLH in northern China can be primarily attributed to latent heat flux (36 %) during the summer season, which effectively explains the impact of vegetation greening on BLH. The substantial increase in greening in northern China stands out as the most significant contributing factor to the reduction in BLH during summer. Consequently, further ecohydrological investigations are crucial for the sustainable environmental development of northern China. Overall, these findings greatly enhance our understanding of the long-term changes in BLH across China and underscore the importance of considering various contributing factors for a comprehensive analysis.

## CRediT authorship contribution statement

**Congcong Li:** Writing – review & editing, Writing – original draft, Visualization, Validation, Methodology, Investigation, Formal analysis, Data curation, Conceptualization. **Xuanze Zhang:** Methodology. **Jianping Guo:** Methodology, Data curation. **Qiang Yu:** Resources, Methodology. **Yongqiang Zhang:** Writing – review & editing, Supervision, Resources, Methodology, Funding acquisition, Conceptualization.

## Declaration of competing interest

The authors declare that they have no known competing financial interests or personal relationships that could have appeared to influence the work reported in this paper.

## Data availability

Data will be made available on request.

## Acknowledgements

This study was supported by the Second Tibetan Plateau Scientific Expedition and Research Program (2019QZKK020807), the National Key R&D Program of China (Grant No. 2022YFC3002804), and the National Natural Science Foundation of China (Grant Nos. 42330506 and 42001019). We appreciate the reviewers and editors for their constructive comments and suggestions. The seasonal *BLH* data used in this study were obtained from the China Meteorological Administration (http://data.cma.cn/en/). The ERA5 daily data supporting this study are freely available at (https://cds.climate.copernicus.eu/). Furthermore, the PML_V2 data are freely available at Google Earth Engine (https://code.earthengine.google.com/?asset=projects/pml_evapotranspiration/PML/OUTPUT/PML_V2_8day_v016). The China meteorological forcing dataset is freely available from (https://data.tpdc.ac.cn/). Last, the LAI product (MOD15A2H.006) supporting this study is freely available at (https://lpdaac.usgs.gov/products/mod15a2hv006/).

## Supplementary materials

Supplementary material associated with this article can be found, in the online version, at doi:10.1016/j.agrformet.2024.109910.

## References

Acs, F., et al., 2014. Sensitivity of WRF-simulated planetary boundary layer height to land cover and soil changes. Meteorol. Z. 23 (3), 279–293.
Beyrich, F., 1997. Mixing height estimation from sodar data - a critical discussion. Atmos. Environ. 31 (23), 3941–3953.
Bian, J., et al., 2011. intercomparison of humidity and temperature sensors: GTS1, Vaisala RS80, and CFH. Adv Atmos Sci 28 (1), 139–146.
Brugger, P., et al., 2018. Effect of surface heterogeneity on the boundary-layer height: a case study at a semi-arid forest. Bound. Layer Meteorol. 169 (2), 233–250.
Cao, B., et al., 2020. Factors influencing the boundary layer height and their relationship with air quality in the Sichuan Basin, China. Sci. Total Environ, 727, 138584.
Chen, c., et al., 2019a. China and India lead in greening of the world through land-use management. Nat. Sustain. 2 (2), 122–129.
Chen, X., et al., 2019b. Tropopause trend across China from 1979 to 2016: a revisit with updated radiosonde measurements. Int. J. Climatol. 39 (2), 1117–1127.
Chen, Y., et al., 2020. To blend or not to blend? A framework for nationwide landsat-MODIS data selection for crop yield prediction. Remote Sens. 12 (10).
Darand, M., Zandkarimi, F., 2019. Identification of atmospheric boundary layer height and trends over Iran using high-resolution ECMWF reanalysis dataset. Theor Appl Climatol 137 (1–2), 1457–1465.
Garratt, J.R., 1994. Review: the atmospheric boundary layer. Earth Sci Rev 37 (1), 89–134.
Guo, J., et al., 2016a. Delaying precipitation and lightning by air pollution over the Pearl River Delta. Part I: observational analyses. J. Geophys. Res. 121 (11), 6472–6488.
Guo, J., et al., 2019. Shift in the temporal trend of boundary layer height in china using long-term (1979–2016) Radiosonde Data. Geophys. Res. Lett. 46 (11), 6080–6089.
Guo, J., et al., 2016b. The climatology of planetary boundary layer height in China derived from radiosonde and reanalysis data. Atmos. Chem. Phys. 16 (20), 13309–13319.
He, J., et al., 2020. The first high-resolution meteorological forcing dataset for land process studies over China. Sci. Data 7 (1).
Helbig, M., et al., 2021. Integrating continuous atmospheric boundary layer and tower-based flux measurements to advance understanding of land-atmosphere interactions. Agric. For. Meteorol. 307, 108509.
Hernandez, C., Drobinski, P., Turquety, S., 2015. Impact of wildfire-induced land cover modification on local meteorology: a sensitivity study of the 2003 wildfires in Portugal. Atmos. Res. 164-165, 49–64.
Hersbach, H., Bell, B., Berrisford, P., Hirahara, S., Thépaut, J., 2020. The ERA5 global reanalysis. Quart. J. R. Meteorol. Soc.
Jousse, A., Hall, A., Sun, F., Teixeira, J., 2016. Causes of WRF surface energy fluxes biases in a stratocumulus region. Clim. Dyn. 46 (1–2), 571–584.
Lawrence, M.G., 2005. The relationship between relative humidity and the dewpoint temperature in moist air: a simple conversion and applications. Bull. Am. Meteorol. Soc. 86 (2), 225–234.
Li, D., et al., 2020. Impacts of land use and land cover changes on regional climate in the Lhasa River basin, Tibetan Plateau. Sci. Total Environ, 742, 140570.
Liang, W., et al., 2015. Quantifying the impacts of climate change and ecological restoration on streamflow changes based on a Budyko hydrological model in China's Loess Plateau. Water Resour. Res. 51 (8), 6500–6519.
Liu, S., Liang, X.-Z., 2010. observed diurnal cycle climatology of planetary boundary layer height. J. Clim. 23 (21), 5790–5809.
Ma, M., Pu, Z., Wang, S., Zhang, Q., 2011. Characteristics and numerical simulations of extremely large atmospheric boundary-layer heights over an arid region in north-west China. Bound. Layer Meteorol. 140 (1), 163–176.
Malavelle, F., et al., 2011. Simulation of aerosol radiative effects over West Africa during DABEX and AMMA SOP-0. J. Geophys. Res. 116.
Mayor, S.D., 2017. Observations of microscale internal gravity waves in very stable atmospheric boundary layers over an orchard canopy. Agric. For. Meteorol. 244-245, 136–150.
Mccumber, M.C., Pielke, R.A., 1981. Simulation of the effects of surface fluxes of heat and moisture in a mesoscale numerical model: 1. Soil layer. J. Geophys. Res.
Miao, Y., et al., 2017. Classification of summertime synoptic patterns in Beijing and their associations with boundary layer structure affecting aerosol pollution. Atmos. Chem. Phys. 17 (4), 3097–3110.
Myneni, R., Knyazikhin, Y., Park, T., 2015. MOD15A2H MODIS/Terra Leaf Area Index/FPAR 8-Day L4 Global 500m SIN Grid V006. NASA EOSDIS Land Processes DAAC.
Ou, J., et al., 2021. Vertical characterization and potential sources of aerosols in different seasons over the Yangtze River Delta using ground-based MAX-DOAS. Environ. Pollut. 279, 116898-116898.
Prueger, J.H., Hipps, L.E., Cooper, D.I., 1996. Evaporation and the development of the local boundary layer over an irrigated surface in an arid region. Agric. For. Meteorol. 78 (3), 223–237.
Qiu, L., et al., 2017. Spatiotemporal response of the water cycle to land use conversions in a typical hilly–gully basin on the Loess Plateau, China. Hydrol. Earth Syst. Sci. 21 (12), 1–30.
Raval, A., Ramanathan, V., 1989. Observational determination of the greenhouse effect. Nature 342 (6251), 758–761.
Rihani, J.F., Chow, F.K., Maxwell, R.M., 2015. Isolating effects of terrain and soil moisture heterogeneity on the atmospheric boundary layer: idealized simulations to diagnose land-atmosphere feedbacks. J. Adv. Model. Earth Syst. 7 (2), 915–937.
Roderick, M.L., Rotstayn, L.D., Farquhar, G.D., Hobbins, M.T., 2007. On the attribution of changing pan evaporation. Geophys. Res. Lett. 34 (17).
Seibert, P., et al., 2000. Review and intercomparison of operational methods for the determination of the mixing height. Atmos Environ 34 (7), 1001–1027.

Seidel, D.J., Ao, C.O., Li, K., 2010. Estimating climatological planetary boundary layer heights from radiosonde observations: comparison of methods and uncertainty analysis. J. Geophys. Res. 115 (D16).
Stull, R.B., 2012. An Introduction to Boundary Layer Meteorology, 13. Springer Science & Business Media.
Su, T., et al., 2017. An intercomparison of long-term planetary boundary layer heights retrieved from CALIPSO, ground-based lidar, and radiosonde measurements over Hong Kong. J. Geophys. Res. 122 (7), 3929–3943.
Sudeepkumar, B.L., Babu, C.A., Varikoden, H., 2020. Atmospheric boundary layer height and surface parameters: trends and relationships over the west coast of India. Atmos. Res. 245, 105050.
Tang, G.Q., et al., 2021. Aggravated ozone pollution in the strong free convection boundary layer. Sci. Total Environ, 788.
Wan, Y., Zhang, Y., Zhang, J., Peng, Y., 2017. Influence of sensible heat on planetary boundary layer height in East Asia. Plateau Meteorol. 36 (1), 173–182.
Wang, G., Chen, X.-Y., Qiao, F.-L., Wu, Z., Huang, N.E., 2010. On Intrinsic mode function. Adv. Adapt. Data Anal. 02 (03), 277–293.
Wang, W., Mao, F., Gong, W., Pan, Z., Du, L., 2016. Evaluating the governing factors of variability in nocturnal boundary layer height based on elastic lidar in Wuhan. Int. J. Environ. Res. Public Health 13 (11).
Wang, Y., Khalizov, A., Levy, M., Zhang, R., 2013. New directions: light absorbing aerosols and their atmospheric impacts. Atmos. Environ. 81, 713–715.
Xu, Z., Chen, H., Guo, J., Zhang, W., 2021a. Contrasting effect of soil moisture on the daytime boundary layer under different thermodynamic conditions in summer over China. Geophys. Res. Lett. 48 (3), e2020GL090989.
Xu, Z.C., Cheng, L., Liu, P., Makarieva, O., Chen, M.H., 2021b. Detecting and quantifying the impact of long-term terrestrial water storage changes on the runoff ratio in the head regions of the two largest rivers in China. J. Hydrol. 601.
Xue, W., et al., 2019. Declining diurnal temperature range in the North China Plain related to environmental changes. Clim. Dyn. 52 (9–10), 6109–6119.
Yang, D., Li, C., Lau, A.K.-H., Li, Y., 2013. Long-term measurement of daytime atmospheric mixing layer height over Hong Kong. J. Geophys. Res. 118 (5), 2422–2433.
Zha, J., Wu, J., Zhao, D., 2017. Effects of land use and cover change on the near-surface wind speed over China in the last 30 years. Prog. Phys. Geogr. 41, 46–67.
Zhang, B.Q., Tian, L., Zhao, X.N., Wu, P.T., 2021. Feedbacks between vegetation restoration and local precipitation over the Loess Plateau in China. Sci. China Earth Sci. 64 (6), 920–931.
Zhang, W., et al., 2017. On the summertime planetary boundary layer with different thermodynamic stability in china: a radiosonde perspective. J. Clim. 31.
Zhang, W., et al., 2016a. Planetary boundary layer height from CALIOP compared to radiosonde over China. Atmos. Chem. Phys. 16 (15), 9951–9963.
Zhang, Y., et al., 2014. On the computation of planetary boundary-layer height using the bulk Richardson number method. Geosci. Model Dev. 7 (6), 2599–2611.
Zhang, Y., et al., 2016b. Multiple afforestation programs accelerate the greenness in the 'Three North' region of China from 1982 to 2013. Ecol. Indic. 61, 404–412.
Zhang, Y., Seidel, D.J., Zhang, S., 2013. Trends in planetary boundary layer height over Europe. J. Clim. 26 (24), 10071–10076.
Zhang, Y., et al., 2023. Future global streamflow declines are probably more severe than previously estimated. Nat. Water 1 (3), 261–271.
Zhang, Y.Q., et al., 2019. Coupled estimation of 500m and 8-day resolution global evapotranspiration and gross primary production in 2002-2017. Remote Sens. Environ. 222, 165–182.
Zhu, X.W., et al., 2018. Mixing layer height on the North China Plain and meteorological evidence of serious air pollution in southern Hebei. Atmos. Chem. Phys. 18 (7), 4897–4910.
Zuidema, P., Painemal, D., de Szoeke, S., Fairall, C., 2009. Stratocumulus cloud-top height estimates and their climatic implications. J. Clim. 22 (17), 4652–4666.